光学学报

基于飞秒激光加工的高阈值高阶贝塞尔光束产生器件

张作蛟[1,2]，方瑶[1]，王青松[1]，李雄[1,2]，蒲明博[1,2,3]，马晓亮[1,2]，罗先刚[1,2*]

[1]中国科学院光电技术研究所微细加工光学技术国家重点实验室，四川 成都 610209；

[2]中国科学院大学，北京 100049；

[3]中国科学院光电技术研究所矢量光场研究中心，四川 成都 610209

摘要 高阶贝塞尔光束能够携带轨道角动量，且具有无衍射特性，在粒子操控、激光微纳加工及非线性光学等领域具有重要应用价值。目前产生高阶贝塞尔光束的方式无法同时满足集成化和高功率场景的应用需求。基于飞秒激光诱导的双折射纳米光栅结构，提出一种高损伤阈值的集成化光场调控器件制备方法。通过调控纳米光栅的光轴方向和相位延迟量，在石英玻璃内部写入光轴取向空间变化的多层纳米光栅结构，制备的器件可以实现不同光场调控功能的叠加和不同工作波长的设计。基于所提方法制备了中心波长为 532 nm、拓扑荷值为 4 的高阶贝塞尔光束产生器件。器件产生的高阶贝塞尔光束携带的轨道角动量与设计值相符，在 4 m 距离内光斑大小保持基本不变。器件的零几率激光损伤阈值为 28.5 J/cm^2(6 ns)，在高功率激光光束整形等领域具有极大的应用潜力。

关键词 激光光场调控；高阶贝塞尔光束；集成化光学元件；飞秒激光；纳米光栅；激光损伤阈值

中图分类号 O436 **文献标志码** A **DOI**：10.3788/AOS230450

1 引 言

涡旋光束是一种具有螺旋形的波前相位 exp(i$l\theta$)并在轴上存在相位奇点的结构光束[1-2]。沿光轴传输时，涡旋光束光场呈现中空的环形分布。高阶贝塞尔光束是一种特殊的涡旋光束，其光斑大小在一定范围内不随传播距离的增加而扩散。高阶贝塞尔光束凭借携带轨道角动量(OAM)特性和无衍射特性[3]，在光镊技术[4-6]、激光微纳加工[7-8]、光学成像[9-10]和非线性光学[11-12]等领域有着广泛的应用。

近年来，如何产生携带轨道角动量的高阶贝塞尔光束成为了科研工作者的研究热点[13-15]。常见的产生器件包括螺旋相位板-锥透镜[16]、空间光调制器[17-18]和超表面[19-20]等。螺旋相位板-锥透镜法使用螺旋相位板产生拉盖尔-高斯(LG)光束，随后再通过锥透镜将 LG 光束转换为高阶贝塞尔光束。此方法在高功率激光光束转换时具有优势，但多器件的组合增加了光学系统的复杂性并限制了光子器件的集成化发展。空间光调制器由液晶阵列构成，通过加载对应的相位信息可灵活地调控贝塞尔光束的参数。但液晶材料的激光损伤阈值(LIDT)通常低于 1 J/cm^2(13 ns)[21]，无法满足高功率的应用场景。超表面器件通过调控单元结构的几何形状和空间位置来操控相位、振幅等电磁参数，从而构建多种平面光学器件[22-27]。此类器件能够实现高集成化的光场调控功能，但器件的激光损伤阈值仍较低[28]。综上所述，如何制备兼顾集成化和高损伤阈值的高阶贝塞尔光束产生器件是当前亟待解决的问题。

本文根据几何相位器件设计原理，基于飞秒激光诱导的亚波长双折射纳米光栅结构，实现了高损伤阈值集成化光场调控器件的制备。采用飞秒激光多层加工的方式，通过精准调控纳米光栅的光轴取向和相位延迟，在石英玻璃内部写入多种光学器件的相位分布，可实现不同光学功能的叠加，得到集成化的光场调制器件。据此，在石英玻璃内分别写入螺旋相位板和锥透镜的相位分布，制备了中心波长为 532 nm、拓扑荷值为 4 的高阶贝塞尔光束产生器件。该器件生成的高阶贝塞尔光束在 4 m 距离内保持了良好的无衍射传输。同时，采用 1-on-1 的方式测得器件在 1064 nm、6 ns 脉冲激光作用下的损伤阈值为 28.5 J/cm^2(6 ns)。基于此方法制备的高损伤阈值、集成化的光束整形器件在激光加工、航空航天等领域有着广阔的应用前景。

收稿日期：2023-01-06；**修回日期**：2023-02-19；**录用日期**：2023-03-12；**网络首发日期**：2023-03-22

基金项目：国家重点研发计划项目(2018YFA0701800)、中国科学院关键技术研发团队项目(GJJSTD20210005)

通信作者：*lxg@ioe.ac.cn

2　纳米光栅结构

2.1　基于纳米光栅结构的几何相位调控

随着飞秒激光微纳加工技术的发展，飞秒激光在透明介质中诱导的亚波长双折射纳米光栅结构引起了人们的广泛关注，并基于纳米光栅结构制备了多种几何相位器件，如衍射光栅、偏振转化器和5D数据存储器件等[29-35]。纳米光栅区域中氧元素的浓度受到周期性调制，缺氧部位的折射率比未改性区域低0.2左右[36]。由于折射率的周期性变化，入射光振动方向垂直和平行于光栅结构的两个分量间产生相位延迟，纳米光栅表现出双折射特性。双折射特性的表征参数主要有两个：光轴角度α和相位延迟量R。纳米光栅作为一种各向异性微纳结构，可以通过改变入射光的偏振状态得到几何相位的变化[37,38]，如图1所示，此过程可通过Jones矩阵描述：

$$\begin{bmatrix} E_{x\mathrm{out}} \\ E_{y\mathrm{out}} \end{bmatrix} = J \begin{bmatrix} E_{x\mathrm{in}} \\ E_{y\mathrm{in}} \end{bmatrix}, \tag{1}$$

$$J = \begin{bmatrix} J_{11} & J_{12} \\ J_{21} & J_{22} \end{bmatrix}, \tag{2}$$

式中：$E_{x\mathrm{out}}$和$E_{y\mathrm{out}}$分别为出射光在x和y方向上的偏振分量；$E_{x\mathrm{in}}$和$E_{y\mathrm{in}}$分别为入射光在x和y方向上的偏振分量；J为Jones矩阵。

假定纳米光栅所在的坐标系主轴方向为u和v，u轴和x轴夹角为α，推导得[26]：

$$J = \begin{bmatrix} t_u \cos^2\alpha + t_v \sin^2\alpha & (t_u - t_v)\sin\alpha\cos\alpha \\ (t_u - t_v)\sin\alpha\cos\alpha & t_u \sin^2\alpha + t_v \cos^2\alpha \end{bmatrix}, \tag{3}$$

式中：t_u和t_v分别为纳米光栅在两个主轴方向上的透射复振幅。当入射光为圆偏振光时，透过光栅结构的出射光可表示为

$$\begin{bmatrix} E_{x\mathrm{out}} \\ E_{y\mathrm{out}} \end{bmatrix} = \frac{J}{\sqrt{2}} \begin{bmatrix} 1 \\ \pm \mathrm{i} \end{bmatrix} = \frac{1}{2\sqrt{2}} \left\{ (t_u + t_v) \begin{bmatrix} 1 \\ \pm \mathrm{i} \end{bmatrix} + (t_u - t_v)\exp(\pm 2\mathrm{i}\alpha) \begin{bmatrix} 1 \\ \mp \mathrm{i} \end{bmatrix} \right\}, \tag{4}$$

式中："±"对应左旋和右旋圆偏振态。可知在圆偏光入射时，出射光为与入射光偏振态相同和相反两个分量的叠加，并且偏振态相反的分量携带了值为光轴角度两倍的几何相位变化：

$$\varphi = \pm 2\alpha。 \tag{5}$$

由此，基于飞秒激光诱导的纳米光栅写入不同的光轴分布即可获得空间变化的几何相位调控功能。调控光轴角度从0～π的连续变化可实现出射光从0～2π的全相位调制。当$t_u + t_v = 0$时，即出射光在纳米光栅快轴和慢轴方向上的振幅相同但相位差为π时，出射光完全转换为与入射光偏振方向相反的圆偏振光，此时纳米光栅结构可视为半波片。

2.2　双折射特性的调控

飞秒激光加工系统主要参数如表1所示，其中，

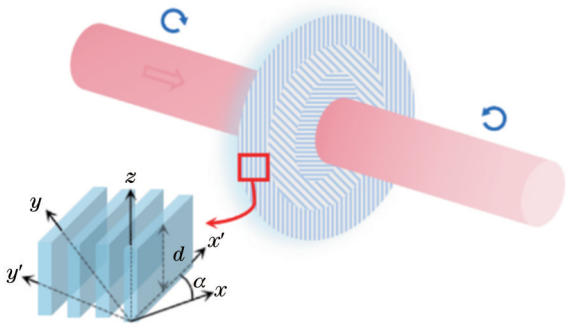

图1　基于纳米光栅结构制备几何相位器件的示意图

Fig. 1　Schematic of the fabrication of geometric phase optical element based on nanograting

A_{NA}表示数值孔径。系统基于中心波长为1030 nm的全光纤飞秒激光器（武汉安扬激光，FemtoYL®系列）搭建而成，如图2(a)所示。激光脉冲能量由半波片（HWP1）结合偏振分光棱镜调控，激光偏振方向由HWP2控制。脉冲激光经物镜（Mitutoyo，M Plan Apo NIR系列）聚焦到石英玻璃（Corning，HPFS 7979）表面以下200～500 μm，聚焦位置由计算机软件控制XYZ三维位移台调节。飞秒激光诱导的纳米光栅是一种周期约为200～300 nm，占空比约为10%的片状结构，如图2(b)所示。纳米光栅的光轴取向和相位延迟可以分别通过激光的偏振方向和加工工艺参数（脉冲能量、脉冲密度和物镜数值孔径等）进行调控。

表1　飞秒激光加工系统主要参数

Table 1　Parameters of femtosecond laser processing system

System parameter	Value
Central wavelength /nm	1030
Repetition frequency /kHz	200
Minimum pulse width /fs	260
Laser polarization direction	Linear polarization(S)
Line interval /μm	1
Focus depth /μm	200-500
Objective	50×(A_{NA}=0.42)

首先研究了飞秒激光诱导的纳米光栅结构随激光偏振方向的演化规律，如图3所示。可以看到，飞秒激光偏振方向从90°连续变化到0°时，纳米光栅的结构取向均垂直于入射激光偏振方向，改变激光偏振方向可以实现光栅光轴的调制。此外，激光偏振方向与扫描方向平行时纳米光栅的结构更加均匀，因此后续加工过程中保持两方向平行以确保光栅结构的光轴和相位延迟量的准确性。

纳米光栅结构的相位延迟可以表示为

$$R = \frac{2\pi}{\lambda} |n_{\mathrm{o}} - n_{\mathrm{e}}| d, \tag{6}$$

式中：λ为测试波长；纳米光栅的双折射系数$\Delta n = |n_{\mathrm{o}} - n_{\mathrm{e}}|$，约为$2\times10^{-3}$～$4\times10^{-3}$。激光加工工艺参数会影响

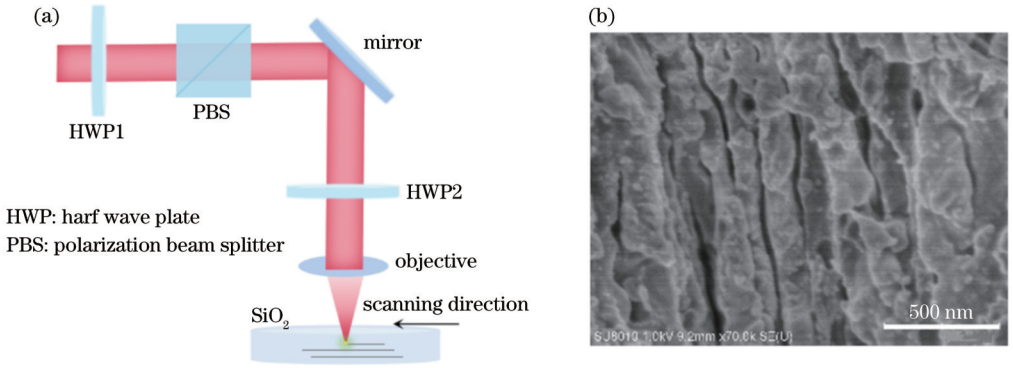

图 2　飞秒激光诱导的纳米光栅结构。(a)飞秒激光加工系统示意图;(b)纳米光栅结构 SEM 图像

Fig. 2　Nanograting structure induced by femtosecond laser. (a) Schematic of the femtosecond laser processing system; (b) SEM image of the nanograting

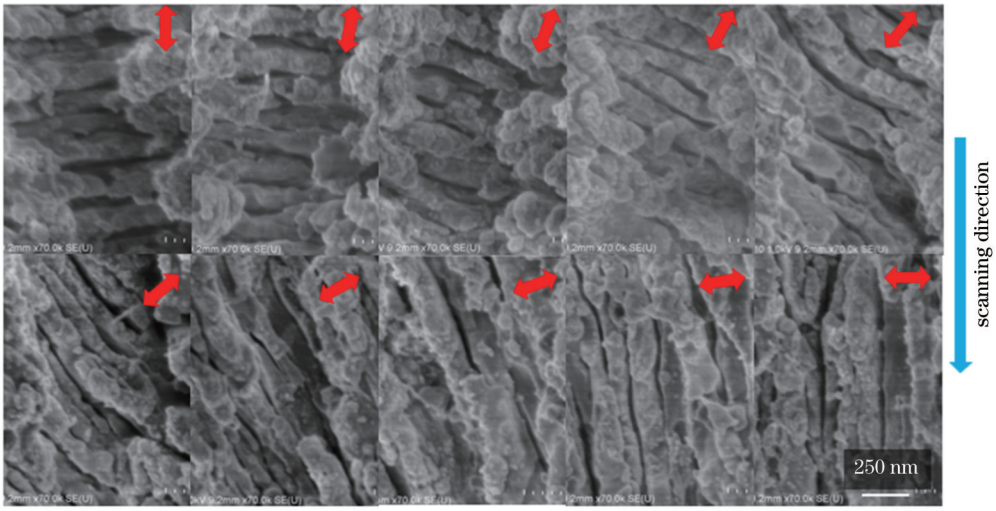

图 3　不同激光偏振方向诱导出的纳米光栅结构的 SEM 图像

Fig. 3　SEM images of nanograting induced by different laser polarization directions

纳米光栅的结构厚度 d,采用不同的工艺参数可以实现纳米光栅相位延迟量的调控。实验时使用 50 倍物镜(A_{NA}=0.42)聚焦激光脉冲,保持飞秒激光重复频率为 200 kHz、脉冲宽度为 260 fs 不变。当脉冲密度(单位长度内的脉冲数量)为 100 pulse/μm、单脉冲能量为 0.3 μJ 时,纳米光栅在不同聚焦深度的平均相位延迟量约为(67.79±1.47) nm,仅需写入 4 层纳米光栅即可达到 532 nm 的半波延迟量,如图 4 所示。

3　实验与讨论

3.1　高阶贝塞尔光束产生器件的相位分布

利用微纳结构对入射光场进行亚波长尺度下的高分辨相位调制是实现复杂光场高效灵活调控的主要方式之一。基于亚波长纳米光栅结构,结合螺旋相位板和平面锥透镜的相位分布对高阶贝塞尔光束产生器件进行设计。高阶贝塞尔光束产生器件的相位分布可以表示为

$$\varphi_{BG}=2\pi r/T+l\theta, \tag{7}$$

式中:r、θ 为极坐标系中的半径和方位角;T 为平面锥透镜的衍射周期。在径向上,器件光轴从 0～π 的突变次数与锥透镜周期相关;角向上,光轴分布仅与拓扑荷值和方位角有关,方位角旋转一周时光轴从 0～π 变化 l 次,可见高阶贝塞尔光束产生器件的功能和相位分布均为螺旋相位板和平面锥透镜两器件的直接相加。

3.2　螺旋相位板和平面锥透镜的测试

基于上述飞秒激光诱导纳米光栅结构的工艺参数,采用多层加工的方式在石英玻璃内部分别制备了拓扑荷值为 4 的螺旋相位板和衍射周期为 0.6 mm 的平面锥透镜,测试结果分别如图 5 和图 6 所示。螺旋相位板的光轴沿角向变化,方位角旋转一周时光轴从 0～π 变化 4 次,与设计相符,如图 5(b)所示。线偏光入射螺旋相位板时,出射光为沿径向或角向偏振的矢量涡旋光束。为检测矢量涡旋光束的偏振状态,需观察矢量涡旋光束经过线偏振片后的光场分布。透射光场为 8 个对称分布的光斑,说明矢量涡旋光束的偏振级数为 4,如图 5(c)所示。光斑间的连线方向与矢量涡旋光束的偏振方向一致,证明了制备的螺旋相位板可以产生矢量涡旋光束。在器件制备过程中,由于脉冲

图 4 加工深度为 200 μm、脉冲能量为 0.3 μJ 时，不同的脉冲密度对纳米光栅相位延迟量的影响

Fig. 4 Effect of different pulse densities on phase retardance of nanograting when the processing depth is 200 μm and the pulse energy is 0.3 μJ

前倾斜效应对飞秒激光能量分布的影响[39,40]，器件存在 4 个对称分布的相位延迟量低于半波延迟约 20 nm 的区域[图 5(a)中箭头所指区域]。在此影响下，如图 5(d)所示，圆偏振光入射时器件生成的涡旋光束光场总体呈空心环形分布，光束中心点的光强基本为零，但存在中心亮斑的光强分布不均匀的问题。进一步检测涡旋光束的 OAM 特性，将涡旋光束与平面光同轴干涉，干涉结果如图 5(e)所示。干涉条纹分叉数为 5，表明涡旋光束的拓扑荷值为 4，且携带着与拓扑荷值相符的 OAM。

贝塞尔光束在激光加工、微粒操纵等领域有着广泛的应用，这些应用往往需要较长的无衍射传输距离。平面锥透镜的无衍射传输距离[41]可表示为

$$Z_{\max}=DT/\lambda, \tag{8}$$

式中：D 为平面锥透镜的通光孔径。可知，入射光束腰宽度不变时，平面锥透镜的最大无衍射传输距离与衍射周期 T 成正比。图 6(c)、(d)分别为入射光束腰宽度为 3.6 mm 时，经平面锥透镜后产生的零阶贝塞尔光束在 2 m 内不同位置的光场分布和径向光强分布。可以看出，零阶贝塞尔光束中心光斑直径约为 250 μm，光斑尺寸和相对光强在传输中基本不变，保持了良好的无衍射特性。

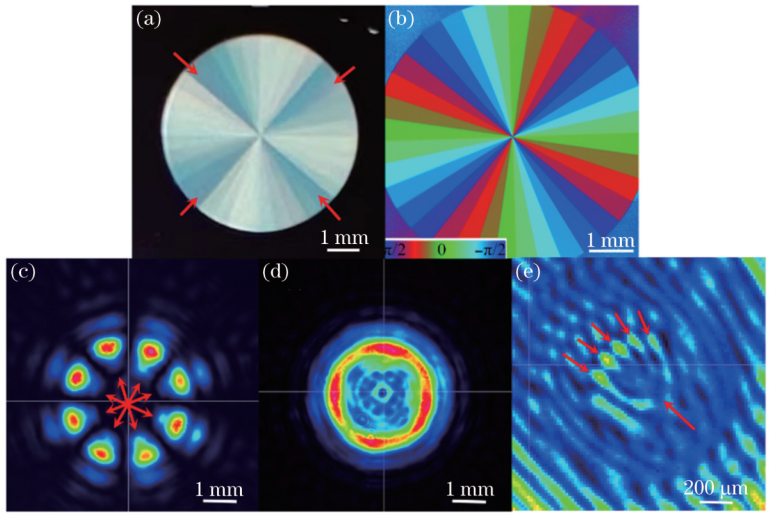

图 5 螺旋相位板的测试结果。(a) 螺旋相位板实物图；(b)螺旋相位板的光轴分布；(c)线偏光入射螺旋相位板时，出射光再经偏振片后的光场分布；(d)圆偏光入射时螺旋相位板产生的涡旋光束；(e)涡旋光束与平面波的干涉图样

Fig. 5 Test results of spiral phase plate. (a) Picture of spiral phase plate; (b) the optical axis distribution of spiral phase plate; (c) the light field distribution of the output passing through the polarizer when the linear polarized light incident on the spiral phase plate; (d) vortex beam generated by circular polarization incident on the spiral phase plate; (e) interference image of vortex beam and plane wave

通过螺旋相位板和锥透镜两个独立的平面器件的制备及测试，验证了基于纳米光栅制备光束整形器件的可行性。由此，借助飞秒激光三维加工能力，利用空间位置将两种器件叠加。先后在石英玻璃内部不同深度写入两种(螺旋相位板和平面锥透镜)共四层光轴取向空间变化的纳米光栅，完成高阶贝塞尔光束产生器件的制备。

3.3 高阶贝塞尔光束产生器件的测试

基于飞秒激光诱导的纳米光栅结构，制备了中心波长为 532 nm、拓扑荷值为 4、衍射周期为 0.6 mm、直径为 6 mm 的高阶贝塞尔光束产生器件。器件的光轴分布与仿真结果一致，光轴的变化沿角向与螺旋相位板相同，沿径向与平面锥透镜相同，如图 7(b)、(c)所示。圆偏光入射时，入射光叠加了螺旋相位板和平面

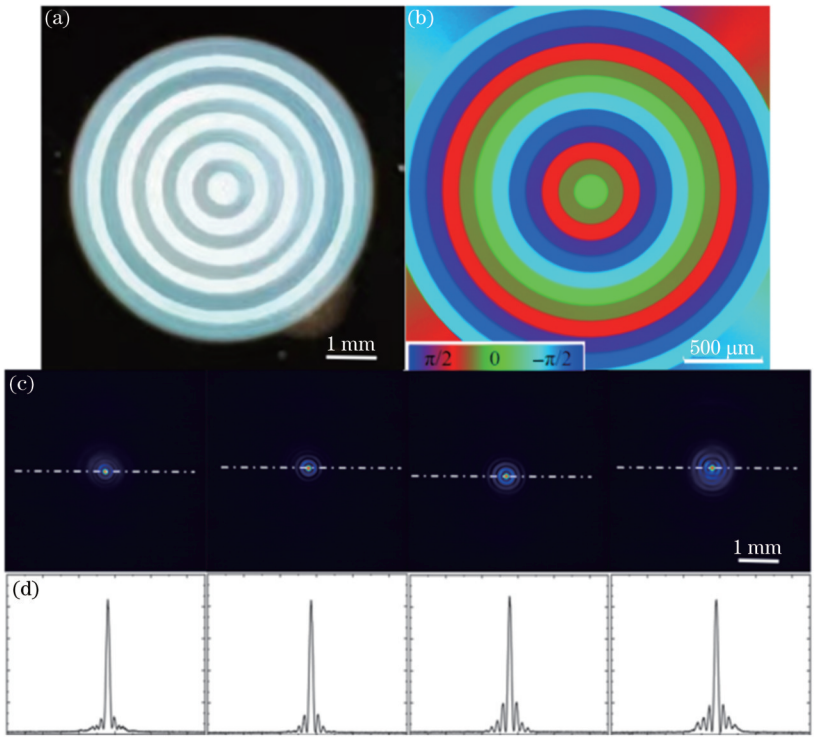

图 6　平面锥透镜的测试结果。(a)平面锥透镜(D=6 mm)实物图;(b)平面锥透镜(D=2.4 mm)的光轴分布;(c)圆偏光入射平面锥透镜(D=6 mm)后,传输距离分别为0.5、1、1.5、2 m时的光场分布;(d)图6(c)对应的光强分布

Fig. 6　Test results of planar axicon. (a) Picture of planar axicon (D=6 mm); (b) the optical axis distribution of planar axicon (D=2.4 mm); (c) the light field distribution measured at 0.5, 1, 1.5, 2 m after the circular polarization incident on planar axicon (D=6 mm); (d) the light intensity distribution in Fig. 6(c)

锥透镜的相位后被调制为高阶贝塞尔光束。在2.5 m处对高阶贝塞尔光束的光场分布进行了测试,如图7(e)所示。高阶贝塞尔光束总体为暗中空的环形分布,由于受到相位延迟量未达半波延迟的区域的影响,高阶贝塞尔光束的中心亮环有所变形且光强分布出现略微偏差。干涉法是检测OAM光束最常用的方法,通过干涉条纹的数量可以判别涡旋光束是否携带与拓扑荷值相符的OAM。将高阶贝塞尔光束分别与球面波和平面波进行同轴干涉,干涉图像如图7(f)、(g)所示。螺旋条纹和叉形条纹数量分别为4和5,均表明高阶贝塞尔光束携带的拓扑荷值为4。

器件的设计衍射周期为0.6 mm、入射光的束腰宽度为3.6 mm时理论无衍射距离为4 m。高阶贝塞尔光束在4 m距离内中心光斑直径保持基本不变,光束的发散角约为1.17 mrad,与测试激光自身发散角(1.2 mrad)相近,可以认为高阶贝塞尔光束在4 m距离内近似无衍射传输,如图8所示。测试距离超过4 m后高阶贝塞尔光束的光斑直径明显扩大。若进一步增加器件的孔径或衍射周期,将获得更远的无衍射传输距离。

为测试器件的抗激光损伤性能,根据ISO 21254激光损伤阈值测试标准,通过标准的1-on-1方法对高阶贝塞尔光束产生器件的激光损伤阈值进行测量。采样点数为12×12,测试波长为1064 nm,脉冲宽度约为6 ns。通过不同能量密度下采样点的损伤概率拟合出零几率损伤的能量密度,即激光损伤阈值,具体如图9所示。测得器件零几率损伤阈值为28.5 J/cm^2,相比于液晶、超构表面等材料或平面器件,基于纳米光栅的几何相位调控器件具有更高的激光损伤阈值,在高功率应用场景下有着更广阔的应用前景。

4　结　　论

基于飞秒激光诱导的纳米光栅结构,提出一种高损伤阈值的光场调控器件的制备方法,实现了集成化高阶贝塞尔光束产生器件的制备。纳米光栅是一种亚波长各向异性双折射结构,其光轴取向和相位延迟可通过激光偏振方向和加工工艺调控。在石英玻璃内部不同深度写入两种(螺旋相位板和平面锥透镜)共四层光轴取向空间变化的纳米光栅,入射光经过多层级联结构后经相位调制产生高阶贝塞尔光束。经测试,器件生成的高阶贝塞尔光束携带与设计值相符的拓扑荷值,并在较长的无衍射传输距离(4 m)内保持光斑大小不变。重要的是,基于纳米光栅的光场调控器件损伤阈值高达28.5 J/cm^2(6 ns),在激光加工等高功率光束整形应用中有较大的优势。所提方法可以将不同功能的光学器件进行集成,为高阈值复杂光场调控器件的集成化制备提供了新思路。

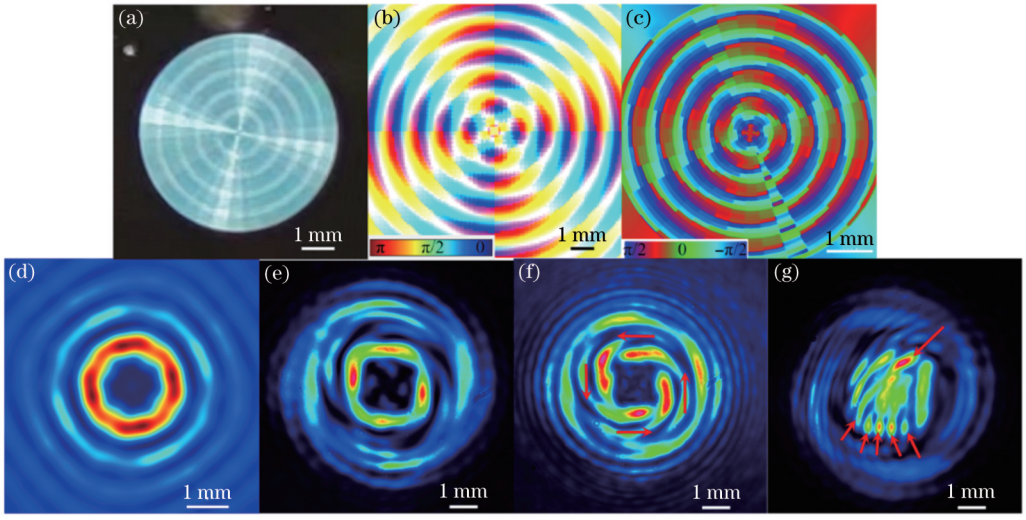

图7 高阶贝塞尔光束产生器件的测试结果。(a)高阶贝塞尔光束产生器件实物图;(b)光轴分布仿真结果;(c)光轴分布测量结果;(d) 2.5 m处光场分布仿真结果;(e) 2.5 m处光场分布测量结果;(f) 高阶贝塞尔光束与球面波干涉结果;(g) 高阶贝塞尔光束与平面波干涉结果

Fig. 7 Test results of high-order Bessel beam generator. (a) Picture of high-order Bessel beam generator; (b) simulation results of optical axis distribution; (c) measurement results of optical axis distribution; (d) simulation results of light field distribution at 2.5 m; (e) measurement results of light field distribution at 2.5 m; (f) interference image of high-order Bessel beam and spherical wave; (g) interference image of high-order Bessel beam and plane wave

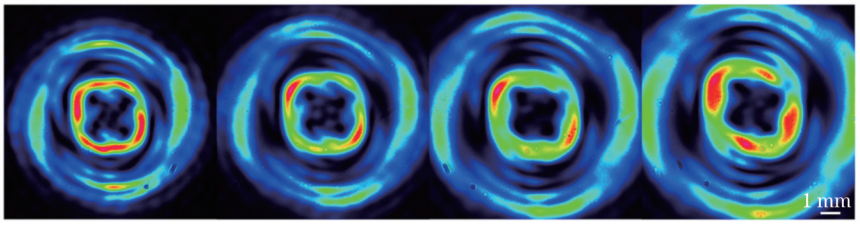

图8 高阶贝塞尔光束的远场测试结果,从左到右测量距离分别为3、3.5、4、4.5 m

Fig. 8 Far field light distribution of high-order Bessel beam, the measured distance is 3, 3.5, 4, 4.5 m from left to right

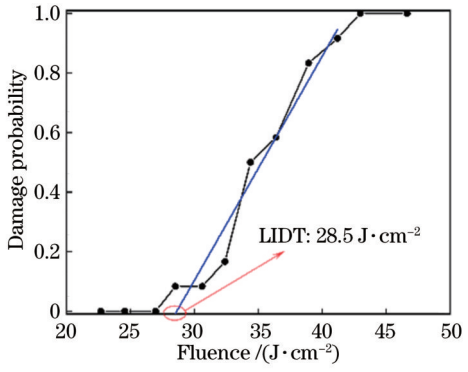

图9 高阶贝塞尔光束生成器件的激光损伤阈值拟合曲线

Fig. 9 LIDT fitting curve of high-order Bessel beam generator

参 考 文 献

[1] Coullet P, Gil L, Rocca F. Optical vortices[J]. Optics Communications, 1989, 73(5): 403-408.

[2] Allen L, Beijersbergen M W, Spreeuw R J, et al. Orbital angular momentum of light and the transformation of Laguerre-Gaussian laser modes[J]. Physical Review A, 1992, 45(11): 8185-8189.

[3] Fahrbach F O, Simon P, Rohrbach A. Microscopy with self-reconstructing beams[J]. Nature Photonics, 2010, 4(11): 780-785.

[4] Grier D G. A revolution in optical manipulation[J]. Nature, 2003, 424(6950): 810-816.

[5] Jeffries G D M, Edgar J S, Zhao Y Q, et al. Using polarization-shaped optical vortex traps for single-cell nanosurgery[J]. Nano Letters, 2007, 7(2): 415-420.

[6] Zhuang X W. Unraveling DNA condensation with optical tweezers[J]. Science, 2004, 305(5681): 188-190.

[7] Kuang Z, Perrie W, Edwardson S P, et al. Ultrafast laser parallel microdrilling using multiple annular beams generated by a spatial light modulator[J]. Journal of Physics D: Applied Physics, 2014, 47(11): 115501.

[8] Ni J C, Wang C W, Zhang C C, et al. Three-dimensional chiral microstructures fabricated by structured optical vortices in isotropic material[J]. Light: Science & Applications, 2017, 6(7): e17011.

[9] Mair A, Vaziri A, Weihs G, et al. Entanglement of the orbital angular momentum states of photons[J]. Nature, 2001, 412(6844): 313-316.

[10] Weber K, Hütt F, Thiele S, et al. Single mode fiber based delivery of OAM light by 3D direct laser writing[J]. Optics Express, 2017, 25(17): 19672-19679.

[11] Wulle T, Herminghaus S. Nonlinear optics of Bessel beams[J]. Physical Review Letters, 1993, 70(10): 1401-1404.

[12] Couairon A, Lotti A, Panagiotopoulos P, et al. Ultrashort laser pulse filamentation with Airy and Bessel beams[J]. Proceedings of SPIE, 2013, 8770: 87701E.

[13] 刘志强, 胡轶瑶, 叶茂. 液晶轴棱锥[J]. 光学学报, 2022, 42(8): 0823001.
Liu Z Q, Hu Y Y, Ye M. Liquid crystal axicon[J]. Acta Optica Sinica, 2022, 42(8): 0823001.

[14] Guo Z M, Liu H H, Xiang L N, et al. Generation of perfect vortex beams with polymer-based phase plate[J]. IEEE Photonics Technology Letters, 2020, 32(10): 565-568.

[15] Shen Y C, Shen Z X, Zhao G Z, et al. Photopatterned liquid crystal mediated terahertz Bessel vortex beam generator[J]. Chinese Optics Letters, 2020, 18(8): 080003.

[16] Arlt J, Dholakia K. Generation of high-order Bessel beams by use of an axicon[J]. Optics Communications, 2000, 177(1/2/3/4/5/6): 297-301.

[17] 李瑞健, 任元, 刘通, 等. 基于纯相位空间光调制器和棋盘相格法制备高阶贝塞尔涡旋光束[J]. 光学学报, 2022, 42(10): 1005001.
Li R J, Ren Y, Liu T, et al. Generation of high-order Bessel beam vortex based on phase-only spatial light modulator and checkerboard phase lattice method[J]. Acta Optica Sinica, 2022, 42(10): 1005001.

[18] Ouadghiri-Idrissi I, Giust R, Froehly L, et al. Arbitrary shaping of on-axis amplitude of femtosecond Bessel beams with a single phase-only spatial light modulator[J]. Optics Express, 2016, 24(11): 11495-11504.

[19] Feng R, Ratni B, Yi J J, et al. Flexible manipulation of Bessel-like beams with a reconfigurable metasurface[J]. Advanced Optical Materials, 2020, 8(23): 2001084.

[20] Li X, Pu M B, Zhao Z Y, et al. Catenary nanostructures as compact Bessel beam generators[J]. Scientific Reports, 2016, 6(1): 1-6.

[21] Lazarev G. Optimization of the liquid crystal on silicon technology for laser microprocessing applications[J]. Physics Procedia, 2016, 83: 1153-1159.

[22] Luo X G, Li X, Pu M B, et al. Symmetric and asymmetric photonic spin-orbit interaction in metasurfaces[J]. Progress in Quantum Electronics, 2021, 79: 100344.

[23] Luo X G, Zhang F, Pu M B, et al. Recent advances of wide-angle metalenses: principle, design, and applications[J]. Nanophotonics, 2021, 11(1): 1-20.

[24] Yu N F, Capasso F. Flat optics with designer metasurfaces[J]. Nature Materials, 2014, 13(2): 139-150.

[25] Li X, Chen L W, Li Y, et al. Multicolor 3D meta-holography by broadband plasmonic modulation[J]. Science Advances, 2016, 2(11): e1601102.

[26] 李雄, 马晓亮, 罗先刚. 超表面相位调控原理及应用[J]. 光电工程, 2017, 44(3): 255-275, 376.
Li X, Ma X L, Luo X G. Principles and applications of metasurfaces with phase modulation[J]. Opto-Electronic Engineering, 2017, 44(3): 255-275, 376.

[27] Wang Y L, Fan Q B, Xu T. Design of high efficiency achromatic metalens with large operation bandwidth using bilayer architecture[J]. Opto-Electronic Advances, 2021, 4(1): 200008.

[28] 崔云, 张晗宇, 赵元安, 等. 飞秒激光作用下金膜的微观特性变化[J]. 中国激光, 2019, 46(2): 0203001.
Cui Y, Zhang H Y, Zhao Y A, et al. Microscopic properties changes of Au film under action of femtosecond laser[J]. Chinese Journal of Lasers, 2019, 46(2): 0203001.

[29] Kazansky P G, Inouye H, Mitsuyu T, et al. Anomalous anisotropic light scattering in Ge-doped silica glass[J]. Physical Review Letters, 1999, 82(10): 2199-2202.

[30] Beresna M, Gecevičius M, Kazansky P G. Polarization sensitive elements fabricated by femtosecond laser nanostructuring of glass[J]. Optical Materials Express, 2011, 1(4): 783-795.

[31] Richter S, Heinrich M, Döring S, et al. Nanogratings in fused silica: formation, control, and applications[J]. Journal of Laser Applications, 2012, 24(4): 042008.

[32] Zhang J Y, Gecevičius M, Beresna M, et al. Seemingly unlimited lifetime data storage in nanostructured glass[J]. Physical Review Letters, 2014, 112(3): 033901.

[33] Drevinskas R, Beresna M, Zhang J Y, et al. Ultrafast laser-induced metasurfaces for geometric phase manipulation[J]. Advanced Optical Materials, 2017, 5(1): 1600575.

[34] 王向贤, 陈函文, 朱剑凯, 等. 金纳米锥阵列与金薄膜耦合结构表面等离子体折射率传感研究[J]. 光电工程, 2022, 49(12): 220135.
Wang X X, Chen H W, Zhu J K, et al. Research on surface plasmon refractive index sensing of gold nano cone array and gold film coupling structure[J]. Opto-Electronic Engineering, 2022, 49(12): 220135.

[35] 欧阳旭, 谢子健, 张孟瑞, 等. 基于激光诱导表面周期结构的微纳防伪结构色[J]. 光电工程, 2022, 49(1): 210320.
Ouyang X, Xie Z J, Zhang M R, et al. Laser-induced periodic surface structure for microscale anti-counterfeiting structural colors[J]. Opto-Electronic Engineering, 2022, 49(1): 210320.

[36] Lancry M, Poumellec B, Canning J, et al. Ultrafast nanoporous silica formation driven by femtosecond laser irradiation[J]. Laser & Photonics Reviews, 2013, 7(6): 953-962.

[37] Balthasar Mueller J P, Rubin N A, Devlin R C, et al. Metasurface polarization optics: independent phase control of arbitrary orthogonal states of polarization[J]. Physical Review Letters, 2017, 118(11): 113901.

[38] Jin J J, Luo J, Zhang X H, et al. Generation and detection of orbital angular momentum via metasurface[J]. Scientific Reports, 2016, 6(1): 1-7.

[39] Kazansky P G, Yang W J, Bricchi E, et al. "Quill" writing with ultrashort light pulses in transparent materials[J]. Applied physics letters, 2007, 90(15): 151120.

[40] Salter P S, Booth M J. Dynamic control of directional asymmetry observed in ultrafast laser direct writing[J]. Applied Physics Letters, 2012, 101(14): 141109.

[41] Yang Q L, Kruk S, Xu Y H, et al. Mie-resonant membrane Huygens′ metasurfaces[J]. Advanced Functional Materials, 2020, 30(4): 1906851.

High-Order Bessel Beam Generator with High Laser-Induced Damage Threshold Fabricated by Femtosecond Laser

Zhang Zuojiao[1,2], Fang Yao[1], Wang Qingsong[1], Li Xiong[1,2], Pu Mingbo[1,2,3], Ma Xiaoliang[1,2], Luo Xiangang[1,2*]

[1]*State Key Laboratory of Optical Technologies on Nano-Fabrication and Micro-Engineering, Institute of Optics and Electronics, Chinese Academy of Sciences, Chengdu* 610209, *Sichuan, China*;

[2]*University of Chinese Academy of Sciences, Beijing* 100049, *China*;

[3]*Research Center on Vector Optical Fields, Institute of Optics and Electronics, Chinese Academy of Sciences, Chengdu* 610209, *Sichuan, China*

Abstract

Objective The high-order Bessel beam (HOBB) is a special kind of vortex beam that carries orbital angular momentum (OAM) and shows non-diffractive and self-healing properties. Thus, HOBBs exhibit great application potential in laser micro/nanofabrication, microparticle manipulation, optical illumination, and nonlinear optics. So far, HOBBs have been generated by several methods, such as traditional optical systems, spatial light modulators, and metasurface. These methods, however, are incapable of achieving both high integrity and high laser-induced damage threshold (LIDT). Based on femtosecond laser-induced birefringent nanograting, a novel method is proposed for the fabrication of integrated optical modulation elements with high LIDT in this work. Multilayer structures with variable phase distribution embedded in silica glass enable the superposition of multiple optical modulation functions for the desired wavelength. For instance, an integrated HOBB generator is fabricated, and the optical modulation characteristics are demonstrated to be consistent with the simulation results. In addition, the LIDT of the fabricated HOBB generator is as high as 28.5 J/cm^2 (6 ns), which has considerable application potential for high-power laser modulation. Consequently, this method can be applied to the fabrication of further integrated optical elements with a high LIDT.

Methods The laser-induced nanograting is an anisotropic structure with birefringent properties. First, the principle of geometric phase modulation is derived based on the birefringent nanograting. The birefringence characteristics of nanograting, including optical axis direction and phase retardance, can be employed to obtain the geometric phase modulation. Second, how the laser processing parameter affects the birefringence of the laser-induced nanograting in silica glass is explored. Then, two independent geometric phase optical elements (GPOEs), including a spiral phase plate (SPP) and a planar axicon, are fabricated and characterized individually. Within silica glass, a multilayer structure with spatially variable optical axis distribution is created by modifying the optical axis direction and phase retardance of nanograting. Finally, the phases of the two GPOEs are integrated. Two forms of nanograting (SPP and planar axicon) with different optical axis distributions are written in separate depths of silica glass. Thus, the incident Gaussian beam is transformed into a HOBB when passing through the multilayer structure. In order to evaluate the laser damage resistance of the prepared optical element, the LIDT is measured by the standard 1-on-1 method (based on the ISO 21254 LIDT test standard).

Results and Discussions When the incident beam is circular polarization, and the retardance of nanograting is half-wave, the output cross-polarized beam will be encoded with a geometric phase change of twice the optical axis angle with high efficiency. The optical axis of the nanograting is perpendicular to the polarization direction of the femtosecond laser (Fig. 3). Therefore, by controlling the polarization direction of the laser, nanograting with spatially variable optical axis directions can be written inside the silica glass. The phase retardance of the nanograting is affected by laser processing parameters. When the laser pulse density is 100 pulse/μm, and the pulse energy is 0.3 μJ, the average retardance of the nanograting is 67.79 ± 1.47 nm at different focusing depths (Fig. 4). In this case, only four layers of the nanograting are required to provide a half-wave retardance of 532 nm. Then, it is demonstrated that the fabricated SPP and planar axicon have excellent optical modulation capability (Fig. 5 and Fig. 6) and that it is feasible to prepare other GPOEs by this method. The interference image shows that the SPP is capable of carrying the OAM of the target value. Over a transmission distance of 2 meters, the planar axicon maintains outstanding non-diffraction properties. After that, the HOBB generated by the integrated element is evaluated (Fig. 7). The light field is typically distributed as a black and hollow ring, with the central ring concentrating the majority of the light intensity. The HOBB carries a topological charge corresponding to its design value of 4. In the non-diffraction distance measurement, the HOBB maintains an almost

constant spot size over a transmission distance of 4 meters (Fig. 8). It is noteworthy that the zero-probability LIDT of the prepared optical element is as high as 28.5 J/cm^2 (6 ns) (Fig. 9), which presents significant benefits in high-power beam shaping applications.

Conclusions In the present study, a method for fabricating an integrated optical modulation element with a high LIDT is proposed and verified. The nanograting is a subwavelength birefringent structure whose optical axis direction and phase retardance can be modified by the laser polarization direction and processing parameters, respectively. The nanograting with spatially variable optical axis distribution can be written inside the silica glass at different depths. The multilayer cascade structure modulates the phase of the incident beam to generate the target beam. Based on the femtosecond laser-induced nanograting, an integrated HOBB generator with an operating wavelength of 532 nm and topological charge of 4 is fabricated. The test results indicate that the optical field modulation performance of the generator is satisfactory. The HOBB generated by the prepared element carries the specified topological charge and keeps spot size constant over a long non-diffraction transmission distance (4 meters). It is crucial that the LIDT of the prepared optical element is as high as 28.5 J/cm^2 (6 ns). This method enables the integration of optical elements with distinct functions, providing a novel concept for the integrated preparation of optical elements with high LIDT and complicated optical field modulation.

Key words laser light field modulation; high-order Bessel beam; integrated optical element; femtosecond laser; nanograting; laser-induced damage threshold